

Article

Bioactive Naphthoquinone and Phenazine Analogs from the Endophytic *Streptomyces* sp. PH9030 as α -Glucosidase Inhibitors

Qingxian Ma ^{1,†}, Yani Zhong ^{1,†}, Pingzhi Huang ^{1,†}, Aijie Li ¹, Ting Jiang ², Lin Jiang ³, Hao Yang ¹, Zhong Wang ¹, Guangling Wu ¹, Xueshuang Huang ^{1,*}, Hong Pu ^{1,*} and Jianxin Liu ^{1,*}

¹ China-Pakistan International Science and Technology Innovation Cooperation Base for Ethnic Medicine Development in Hunan Province, Hunan Provincial Key Laboratory for Synthetic Biology of Traditional Chinese Medicine, School of Pharmaceutical Sciences, Hunan University of Medicine, Huaihua 418000, China; 17608470326@163.com (Q.M.); 18874880070@163.com (Y.Z.); 19918037381@163.com (P.H.); 15274565209@163.com (A.L.); 15274519389@163.com (H.Y.); 13773980672@163.com (Z.W.); guangling2024@126.com (G.W.)

² Jiangxi Drug Inspection Center, Nanchang 330029, China; 15708182636@163.com

³ Hunan Engineering Technology Research Center for Bioactive Substance Discovery of Chinese Medicine, School of Pharmacy, Hunan University of Chinese Medicine, Changsha 410208, China; jianglin@hnuucm.edu.cn

* Correspondence: xueshuanghuang@126.com (X.H.); ph0745@126.com (H.P.); liujianxin3385@126.com (J.L.)

[†] These authors contributed equally to this work.

Abstract: A talented endophytic *Streptomyces* sp. PH9030 is derived from the medicinal plant *Kadsura coccinea* (Lem.) A.C. Smith. The undescribed naphthoquinone naphthgeranine G (**5**) and seven previously identified compounds, **6–12**, were obtained from *Streptomyces* sp. PH9030. The structure of **5** was identified by comprehensive examination of its HRESIMS, 1D NMR, 2D NMR and ECD data. The inhibitory activities of all the compounds toward α -glucosidase and their antibacterial properties were investigated. The α -glucosidase inhibitory activities of **5**, **6**, **7** and **9** were reported for the first time, with IC_{50} values ranging from 66.4 ± 6.7 to 185.9 ± 0.2 μ M, as compared with acarbose ($IC_{50} = 671.5 \pm 0.2$ μ M). The molecular docking and molecular dynamics analysis of **5** with α -glucosidase further indicated that it may have a good binding ability with α -glucosidase. Both **9** and **12** exhibited moderate antibacterial activity against methicillin-resistant *Staphylococcus aureus*, with minimum inhibitory concentration (MIC) values of 16 μ g/mL. These results indicate that **5**, together with the naphthoquinone scaffold, has the potential to be further developed as a possible inhibitor of α -glucosidase.

Keywords: *Kadsura coccinea*; *Streptomyces*; naphthoquinone; phenazine; α -glucosidase inhibitor



Citation: Ma, Q.; Zhong, Y.; Huang, P.; Li, A.; Jiang, T.; Jiang, L.; Yang, H.; Wang, Z.; Wu, G.; Huang, X.; et al. Bioactive Naphthoquinone and Phenazine Analogs from the Endophytic *Streptomyces* sp. PH9030 as α -Glucosidase Inhibitors. *Molecules* **2024**, *29*, 3450. <https://doi.org/10.3390/molecules29153450>

Academic Editor: Brindusa Tipericiu

Received: 1 July 2024

Revised: 19 July 2024

Accepted: 20 July 2024

Published: 23 July 2024



Copyright: © 2024 by the authors. Licensee MDPI, Basel, Switzerland. This article is an open access article distributed under the terms and conditions of the Creative Commons Attribution (CC BY) license (<https://creativecommons.org/licenses/by/4.0/>).

1. Introduction

Diabetes mellitus refers to a group of metabolic illnesses that are characterized by abnormally high amounts of glucose in the bloodstream [1]. The global diabetes population is anticipated to exceed 1.3 billion by 2050 [2]. Type 2 diabetes mellitus (T2DM) is the most prevalent type of diabetes and is found on every continent [3]. α -Glucosidase inhibitors are the most effective medications for treating type 2 diabetes mellitus [4]. Currently, the genus *Streptomyces* is the leading developer of novel and advanced secondary metabolites [5]. Acarbose, derived from a strain of the *Streptomyces* genus, was the first α -glucosidase inhibitor to receive approval in Europe and the U.S. for the treatment of type 2 diabetes [6–8]. Voglibose is a synthetic derivative of N-substituted valiolamine produced by *Streptomyces hygroscopicus* and was chosen as a possible α -glucosidase inhibitor in 1994 [9]. In 1996, miglitol, a synthetic form of nojirimycin produced by *Streptomyces roseochromogenes*, was discovered to be a possible inhibitor of α -glucosidase [10]. It is believed that *Streptomyces* is a major source of α -glucosidase inhibitors.

Naphthoquinone, an important class of natural products derived from microorganisms, exhibits interesting biological activities [11–14]. The naphthgeranines, naphtherpins, and marinones are meroterpenoid families that share a similar naphthoquinone ring structure and have cyclized C-3 geranyl or farnesyl side chains [15]. For example, naphthgeranine B (Figure 1, 1), which was isolated in 1990 from soil-derived *Streptomyces* sp. KO-3988, exhibited a potent cytotoxic effect on HeLa S3 cells ($IC_{50} = 1.6 \mu\text{g/mL}$) [16]. In 1992, marinone (Figure 1, 2), which is isolated from the marine-derived *Streptomyces* sp. CNB-632, was demonstrated to exhibit inhibitory effects against *Bacillus subtilis*, with MIC of $1 \mu\text{g/mL}$ [17]. Phenazines are a diverse collection of secondary metabolites with redox activity that are synthesized by several types of bacteria, such as *Streptomyces* and *Pseudomonas*, as well as by *Methanosarcina* species [18]. The fundamental composition of phenazines consists of a pyrazine ring (1,4-diazabenzene) that contains two interconnected benzene rings [19]. Kankanamge et al. discovered two new dimeric phenazine glycosides, tepuazines A and B, and three new monomeric phenazine glycosides, tepuazines C–E, from the metabolites of *Streptomyces virginiae* CMB-CA091 [20]. Several phenazines possess antimicrobial, antifungal, insecticidal and anticancer properties [21–26]. 2-Bromo-1-hydroxyphenazine (Figure 1, 3), a phenazine compound obtained from a marine-derived *Streptomyces* species, has been shown to possess antibacterial properties against *Staphylococcus aureus* ATCC 25923 and *Staphylococcus epidermidis* ATCC 12228 with MIC values of $1.72 \mu\text{g/mL}$ for both bacteria [27]. 5-Methyl phenazine-1-carboxylic acid (Figure 1, 4), which is obtained from the bacterium PUW5, showed a specific ability to kill lung (A549) and breast (MDA MB-231) cancer cells with IC_{50} values of $488.7 \pm 2.52 \text{ nM}$ and $458.6 \pm 2.48 \text{ nM}$ for lung and breast cancer cells, respectively [28].

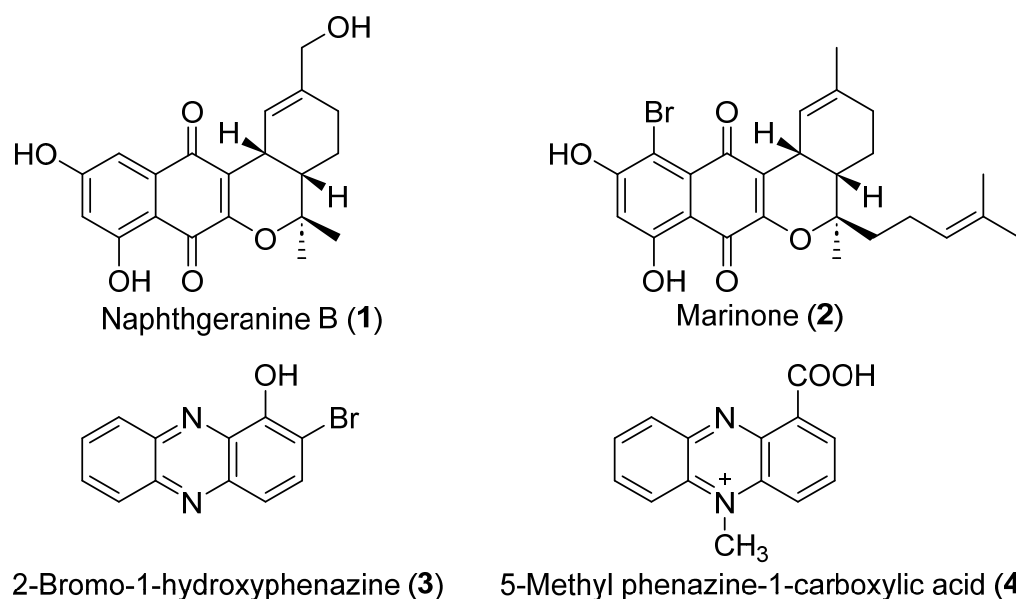


Figure 1. Chemical structures of the naphthoquinone derivatives 1–2 and the phenazine derivatives 3–4.

Kadsura coccinea (Lem.) A.C. Smith (Figure 2A), “黑老虎” in Chinese, is a perennial climbing shrub of the *Schisandraceae* family, known for its medicinal properties. The roots and stems of this plant are used in traditional Chinese medicine for the treatment of gastroenteric diseases, rheumatism, trauma and pain [29,30]. To the best of our knowledge, only a few reports of endophytes and the natural products that they produce from *K. coccinea*. In our continuous exploration of *Streptomyces* natural products [31–33], we have started a project to isolate natural products from endophytic *Streptomyces* strains found in the rhizosphere soil and roots of *K. coccinea*. In this study, we report the isolation of *Streptomyces* from *K. coccinea* (Figure 2B), and that bioactivity-guided natural product isolation

has yielded eight compounds including a new naphthoquinone derivative, naphthgeranine G (Figure 3A, 5), together with two known naphthoquinone derivatives (Figure 3A, 6–7) and five known phenazine derivatives (Figure 3A, 8–12). The ability of these compounds to inhibit α -glucosidase was tested. The data obtained suggest that the majority of these compounds exhibited significant inhibitory effects on α -glucosidase. Among these, 5 exhibited the strongest inhibition, with an IC_{50} value of $66.4 \pm 6.7 \mu\text{M}$. Molecular docking and molecular dynamics studies were performed to further investigate the interaction, orientation and conformation of 5 over the active site of α -glucosidase. Therefore, 5 is a potential α -glucosidase inhibitor. Furthermore, the evaluation of antibacterial activity revealed that both 9 and 12 had moderate antibacterial activity against methicillin-resistant *Staphylococcus aureus* (MRSA), with MIC values of $16 \mu\text{g/mL}$.

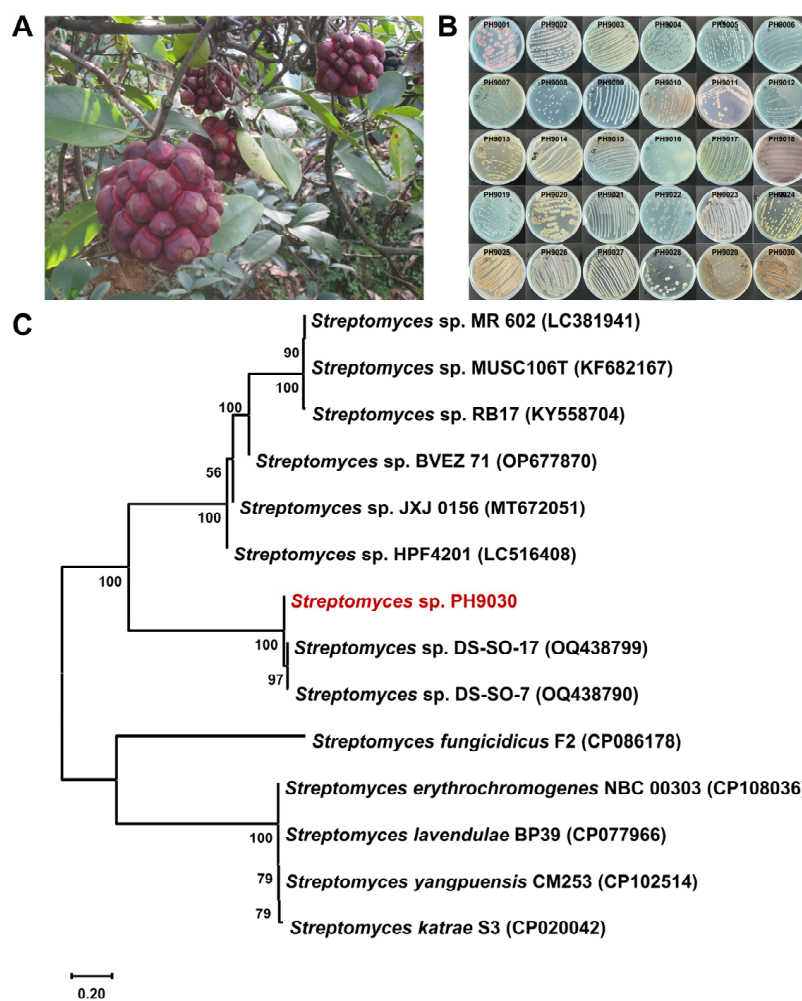


Figure 2. Source of *Streptomyces*. (A) The whole plant of *K. coccinea*. (B) Morphological characterization of actinobacterial isolates. Colony morphology of different actinobacterial isolates derived from the medicinal plant *K. coccinea*. (C) Phylogenetic tree analysis of *S. sp. PH9030* (red).

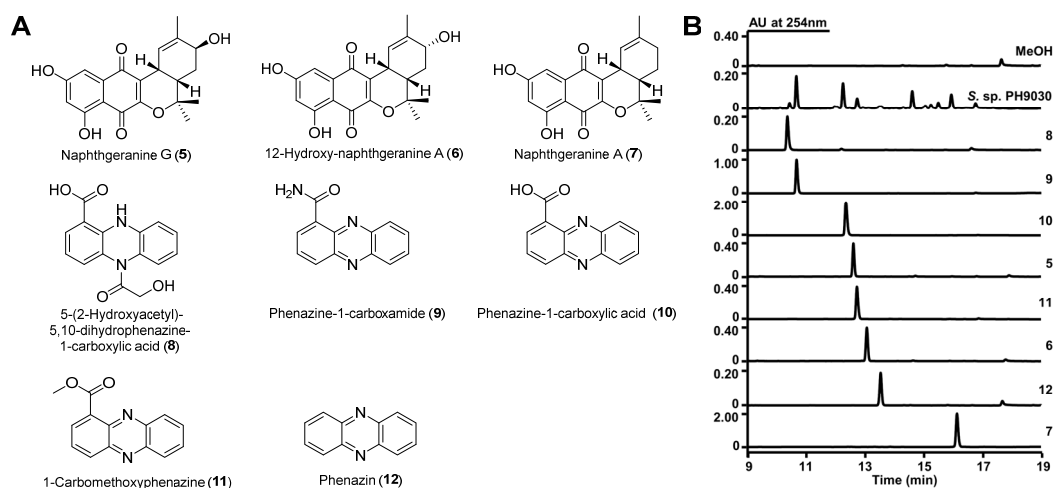


Figure 3. (A) Compounds 5–12 isolated from *S. sp. PH9030*; (B) HPLC analysis of crude extracts and isolated compounds from *S. sp. PH9030*. UV absorption was monitored at 254 nm.

2. Results and Discussion

2.1. Actinomycete Isolation, Small-Scale Fermentation and Antibacterial Activity Assay

Thirty isolates, designated PH9001–PH9030 (Figure 2B), were obtained from the rhizosphere soil and roots of the medicinal plant *K. coccinea*. The plant samples were collected from a mountain ditch in Tongdao County, Huaihua City, Hunan Province, China (Figure 2A). The isolates were obtained through a series of repeated pure cultures on three different agar media (Table S1, MH14, MH15 and MH16). The morphological characteristics of most of the selected isolates are shown in Figure 2B. For further fermentation and antibacterial activity testing, 18 isolates were selected on the basis of their unique characteristics. The most prevalent secondary metabolites of PH9030 in MH18 medium (Table S1) are shown in Figure S1, where they also strongly inhibited MRSA and *Staphylococcus aureus* ATCC 29213 (Table S2, Figures S1 and S2). As a result, the strain PH9030 was chosen for further study.

2.2. Identification and Phylogenetic Analysis of Strain PH9030

The partial 16S rRNA gene sequences (Figure S3) were identified, and a phylogenetic tree was constructed via the BLAST tool of the NCBI for the molecular identification of PH9030. These findings indicate that PH9030 is a member of the *Streptomyces* genus. The phylogenetic tree constructed using 16S rRNA sequences (GenBank ID: PP593435) indicates that *Streptomyces sp. PH9030* exhibits a significant resemblance to *Streptomyces sp. DS-SO-17* (OQ438799) and *Streptomyces sp. DS-SO-7* (OQ438790) (Figure 2C). Consequently, larger-scale liquid fermentation of *S. sp. PH9030* (123 L) was subsequently used to extract natural compounds and assess their effectiveness in inhibiting α -glucosidase and combating bacterial growth.

2.3. Structure Elucidation

The crude extract of *S. sp. PH9030* was fractionated via several techniques including silica gel, MCI gel CHP20, Sephadex LH-20 chromatography and semipreparative HPLC. This process resulted in the isolation of the compounds 5–12, as shown in Figure 3A,B. 12-Hydroxy-naphthgeranine A (6), naphthgeranine A (7), 5-(2-hydroxyacetyl)-5,10-dihydrophenazine-1-carboxylic acid (8), phenazine-1-carboxamide (9), phenazine-1-carboxylic acid (10), 1-carbomethoxyphenazine (11) and phenazin (12) are known compounds, and their structures were established on the basis of comparisons of their 1D and 2D NMR spectra, HRESIMS data and UV spectra with the literature [34–38] (Figures 3A and S15–S62). Phenazine-1-carboxylic acid (PCA, 10) is a physiologically active chemical that has the po-

tential to prevent and control crop diseases. In 2011, the Ministry of Agriculture of China recognized “Shenzimycin” as a pesticide [23,39].

Naphthgeranine G (**5**) was isolated as a yellow powder. Its molecular formula was established as $C_{20}H_{20}O_6$ on the basis of (–)-HRESIMS analysis (Figure S12) at m/z 355.1177 $[M - H]^-$ (calcd for $C_{20}H_{19}O_6$, 355.1187), suggesting eleven degrees of unsaturation. The ^{13}C NMR spectrum of **5** (Table 1), DEPT-135 and DEPT-90 revealed a total of twenty signals containing two ester carbonyls (δ_C 184.2, 178.5), three phenolic carbons (δ_C 164.9, 164.8, 65.3), six nonprotonated carbons (δ_C 154.3, 136.5, 134.0, 123.0, 107.6, 79.8), three olefinic methine carbons (δ_C 136.5, 120.1, 104.3), two methine carbons (δ_C 33.9, 30.8), one methylene carbon (δ_C 29.4) and three methyl carbons (δ_C 25.5, 24.7, 21.2) (Figures S4). The 1H NMR spectrum (Table 1) also indicated the presence of three sp^2 methines [δ_H 6.64 (1H, s, H-5), 6.10 (1H, d, $J = 4.8$ Hz, H-7) and 6.03 (1H, s, H-10)], three methines [δ_H 3.75 (1H, m, H-12), 3.42 (1H, m, H-9) and 2.04 (1H, ddd, $J = 13.2, 6.2, 2.9$ Hz, H-14)], one methylene [δ_H 1.83 (1H, dd, $J = 13.6, 2.7$ Hz, H-13) and 1.23 (1H, m, H-13)] and three methyl groups [δ_H 1.69 (3H, s, H-16), 1.42 (3H, s, H-17) and 1.26 (3H, s, H-18)]. The 1H and ^{13}C NMR data of **5** are similar to those of 12-hydroxy-naphthgeranine A previously isolated from *Streptomyces* sp. XZYN-4 [34]. This was confirmed by the HMBC correlations from H-9 to C-2 (δ_C 154.3), C-3 (δ_C 123.0), C-10 (δ_C 120.1), C-11 (δ_C 136.5), C-13 (δ_C 29.4) and C-14 (δ_C 33.9), H-13 to C-9 (δ_C 30.8), C-11 (δ_C 136.5), C-12 (δ_C 65.3) and C-15 (δ_C 79.8), H-14 to C-15 (δ_C 79.8), C-12 (δ_C 65.3), C-9 (δ_C 30.8) and C-13 (δ_C 29.4), H-16 to C-10 (δ_C 120.1), C-11 (δ_C 136.5) and C-12 (δ_C 65.3), H-17 to C-14 (δ_C 33.9), C-15 (δ_C 79.8) and C-18 (δ_C 24.7) and H-18 to C-14 (δ_C 33.9), C-15 (δ_C 79.8) and C-17 (δ_C 25.5). The sequence from H-10 to H-12 through H-9, H-14 and H-13 was revealed using the COSY spectrum (Figure 4A). Electronic circular dichroism (ECD) calculations were subsequently employed to determine the absolute configuration of **5** by comparing the ECD spectra of (9R, 12S, 14S)-**5** and (9S, 12R, 14R)-**5** with the experimental results, which suggested a (9R, 12S, 14S)-**5** configuration (Figure 4B). Accordingly, the structure of **5** was elucidated as depicted in Figure 4.

Table 1. 1H NMR (600 MHz) and ^{13}C NMR (150 MHz) data of naphthgeranine G (**5**) in $DMSO-d_6$ (δ in ppm, J in Hz).

Position	Naphthgeranine G (5)	
	δ_C , Type	δ_H (J in Hz)
1	178.5, C	
2	154.3, C	
3	123.0, C	
4	184.2, C	
4a	134.0, C	
5	105.9, CH	6.64 (s)
6	164.9, C	
7	104.3, CH	6.10 (d, 4.8)
8	164.8, C	
8a	107.6, C	
9	30.8, CH	3.42 (m)
10	120.1, CH	6.03 (s)
11	136.5, C	
12	65.3, CH	3.75 (m)
13	29.4, CH ₂	1.83 (dd, 2.7, 13.6); 1.23 (m)
14	33.9, CH	2.04 (ddd, 2.9, 6.2, 13.2)
15	79.8, C	
16	21.2, CH ₃	1.69 (s)
17	25.5, CH ₃	1.42 (s)
18	24.7, CH ₃	1.26 (s)

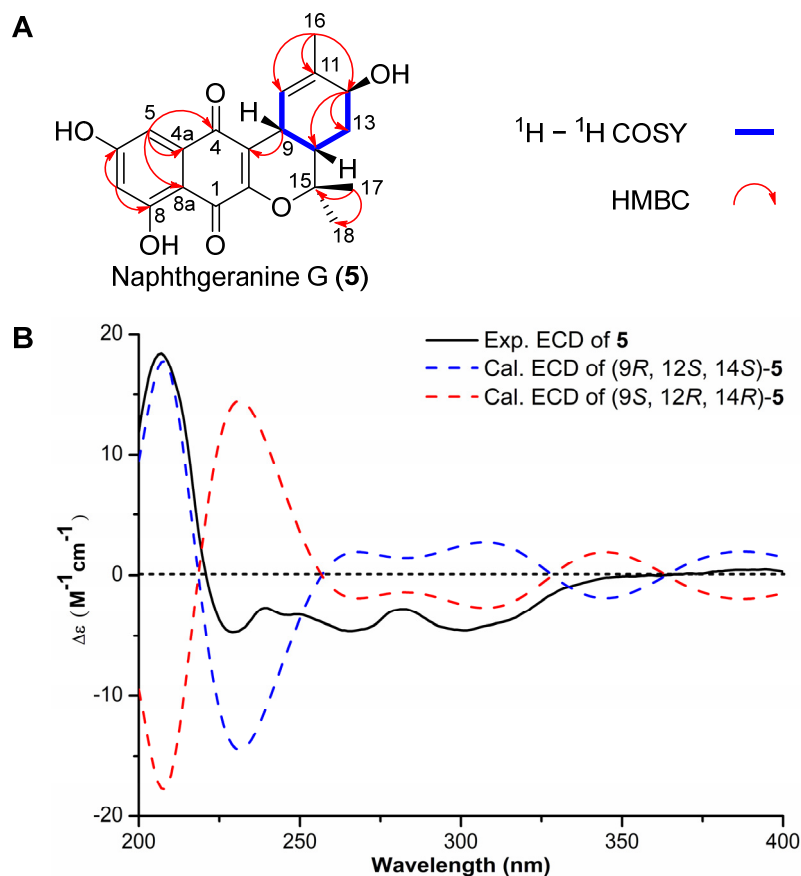


Figure 4. (A) Key ^1H - ^1H COSY and HMBC correlations of compound **5**. (B) Experimental and calculated ECD spectra of the compound **5** in MeOH.

2.4. In Vitro α -Glucosidase Inhibitory Activity

The in vitro α -glucosidase inhibitory activities of the compounds **5**–**12** were assessed. The α -glucosidase inhibitory activities of **5**, **6**, **7** and **9** were reported for the first time, with IC_{50} values ranging from 66.4 ± 6.7 to 185.9 ± 0.2 μM . Acarbose was used as a positive control, and the results are summarized in Table 2. These findings demonstrated that the majority of the compounds had a very promising α -glucosidase inhibitory activity. Notably, **5** exhibited the highest potency ($\text{IC}_{50} = 66.4 \pm 6.7$ μM), surpassing the activity of acarbose ($\text{IC}_{50} = 671.5 \pm 0.2$ μM). The investigation of the structure-activity connection revealed that the presence of C12-OH greatly enhances the molecular framework of α -glucosidase inhibitory activity. Furthermore, the 12*S*-conformation exhibits greater strength than the 12*R*-conformation.

Table 2. α -Glucosidase inhibitory activity of the compounds **5**–**12**.

Compounds	IC_{50} (μM) ^a	Compounds	IC_{50} (μM) ^a
5	66.4 ± 6.7	10	>800
6	115.6 ± 4.4	11	NA ^b
7	185.9 ± 0.2	12	NA ^b
8	NA ^b	Acarbose	671.5 ± 0.2
9	105.4 ± 10.5		

^a Data are presented as means \pm SDs; ^b NA: not active.

2.5. Molecular Docking Simulations of **5** with α -Glucosidase

The software AutoDock Vina 1.1.2 was used for molecular docking research to investigate the interactions between **5**–**12** and α -glucosidase. These compounds, with binding energies greater than that of acarbose, had blocking effects, whereas the compounds with

binding energies lower than acarbose had no activity. These findings matched the results of the experiments (Tables 2 and S6). Owing to its outstanding α -glucosidase inhibitory action, **5** was our primary focus. Figure 5 shows the molecular docking models of **5**. The docking results revealed that **5** formed four hydrogen bonds with Asp-203, Arg-202, Thr-205 and Asn-449 and three hydrophobic interactions with Asp-542, Phe-575 and Tyr-299 (Figure 5). Additionally, to compare the various interactions, we performed molecular docking of acarbose (Figure S63). The affinities of the mentioned inhibitors were calculated, and the results revealed that acarbose has a binding energy of 6.7 kcal/mol and that **5** has a binding energy of 7.2 kcal/mol (Table 3). The docking findings suggested that, compared with acarbose, **5** had a stronger influence on the binding contacts with the active pocket of α -glucosidase, impacting its inhibitory activity.

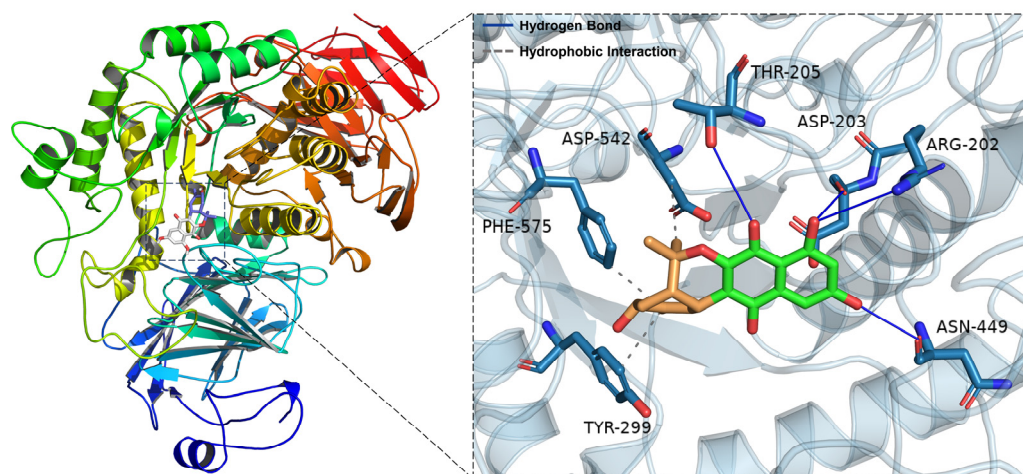


Figure 5. Docking poses and interactions of **5** with α -glucosidase (PDB ID: 2QMJ).

Table 3. Logarithms of free binding energies (FBE, kcal/mol) of naphthgeranine G (**5**) and acarbose to the active cavities of α -glucosidase (PDB ID: 2QMJ) and targeting residues of the binding site located on the mobile flap.

Compound	$-\log(\text{FBE})$	Targeting Residues
Naphthgeranine G (5)	−7.2	Phe-575, Asp-542, Thr-205 Asp-203, Arg-202, Asn-449, Tyr-299
Acarbose	−6.7	Trp-406, Tyr-299, Tyr-605 Thr-205, Arg-526, Asp-443

2.6. Molecular Dynamics Simulations

A molecular dynamics simulation was subsequently conducted under physiologically simulated circumstances to elucidate the binding pattern, stability and molecular interaction mode of **5** with the α -glucosidase protein complex. Structural stability is often assessed on the basis of the presence of low root-mean-square deviation (RMSD) and root-mean-square fluctuation (RMSF) values [40]. The RMSD fluctuation graphs throughout the simulation display the RMSD of the two systems, α -glucosidase/acarbose and α -glucosidase/naphthgeranine G (**5**), as shown in Figure 6A. In the first five ns of the simulation, the two systems converge gradually. In the subsequent simulations, the systems maintain relatively stable fluctuations, with the RMSD keeping the fluctuations between 1 and 2 Å. On the basis of their steady fluctuations, the two systems are stable together. As shown in Figure 6B, all proteins had minimal RMSF values after binding tiny ligands, indicating a solid core structure. Consequently, these proteins are more rigid when bound to small molecules, resulting in the inhibitory action of these small molecules. Significantly, there is a substantial overlap between the red line and the blue line, suggesting that the two tiny chemicals have comparable impacts on the proteins. The radius of gyration (RoG) is a mea-

sure of the compactness of a system and may indicate the degree of densification. Figure 6C clearly shows that the α -glucosidase/acarbose and α -glucosidase/naphthgeranine G (5) systems exhibit similar binding effects and vacillate accordingly. A thorough investigation revealed that the RoG of α -glucosidase/naphthgeranine G (5) mostly decreased during the simulation. This finding indicates that the system became more condensed, suggesting a higher level of binding affinity.

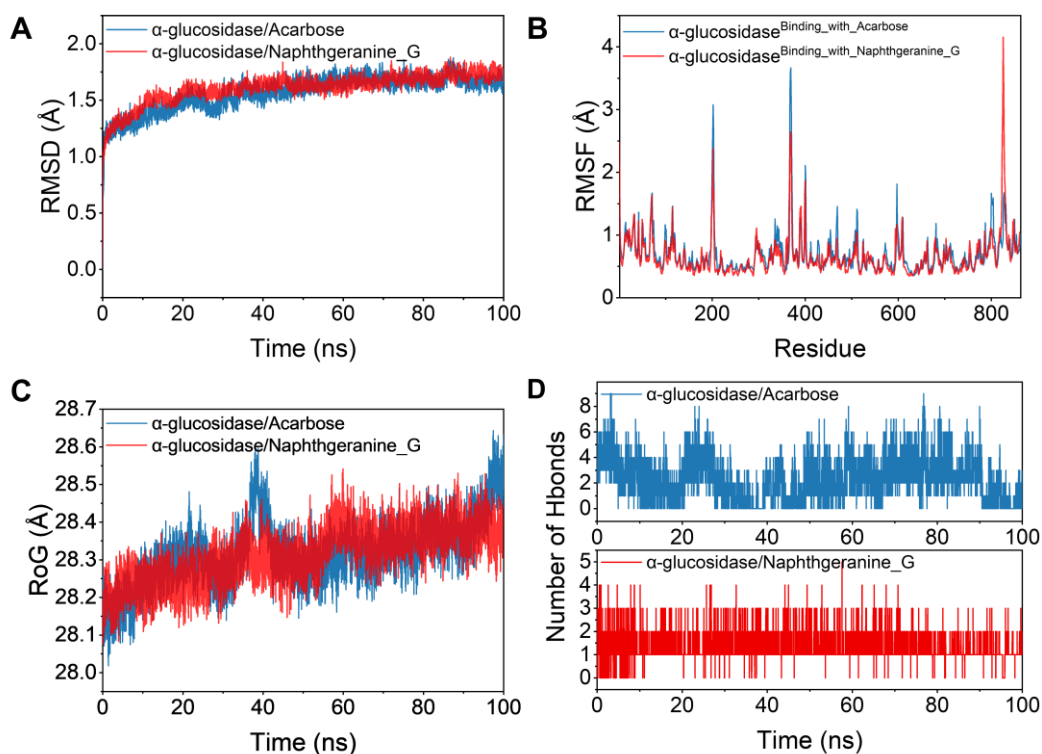


Figure 6. Molecular dynamics of acarbose and 5 with residues in the active pocket of α -glucosidase. (A) The RMSD values of the complex and protein backbone systems were calculated throughout the dynamic simulation. (B) RMSF changes the shapes of the residues that bond in both free proteins and complicated systems. (C) The gyration radius of the four systems was measured during the molecular dynamics simulation. (D) The quantity of hydrogen bonds present in the molecular dynamics simulation.

To better represent the binding modalities of small molecules and target proteins, we computed the binding energies via the MM-GBSA approach, which is based on the trajectories of the molecular dynamic simulations. According to Table S5, the binding energy of the α -glucosidase/acarbose complex was -11.8 ± 4.0 kcal/mol, and that of the α -glucosidase/naphthgeranine G (5) complex was -16.6 ± 1.4 kcal/mol. Smaller values suggest stronger binding, and negative values suggest that the two molecules may bind to the target proteins. Our calculations indicate that α -glucosidase/naphthgeranine G (5) binds more effectively and has a marginally lower value than acarbose. One of the stronger noncovalent ways to bind is through hydrogen bonds, and having more hydrogen bonds results in better binding. Figure 6D shows that the number of hydrogen bonds between α -glucosidase and acarbose remained between one and nine and mostly changed between three and four. These findings suggest that hydrogen bonds are important for keeping the binding of acarbose stable. Hydrogen bonding is among the strongest noncovalent binding interactions, and a greater number of hydrogen bonds indicates better binding. The number of hydrogen bonds in the α -glucosidase/naphthgeranine G (5) complex changed considerably over the simulation period (0–5) but mostly remained at 1–2. These findings suggest that hydrogen bonding plays a minor role in the interaction between α -glucosidase

and naphthgeranine G (5). In summary, naphthgeranine G (5) binds to α -glucosidase more effectively than acarbose. This is in line with the observed experimental findings.

2.7. Antibacterial Activities of 5–12

The MIC values of 5–12 against *Staphylococcus aureus* ATCC 29213, MRSA, *Klebsiella pneumoniae* ATCC 13883 and *Pseudomonas aeruginosa* ATCC 9027 were determined via a broth dilution assay in 96-well plates, with levofloxacin as a control (Table S7). Both 9 and 12 demonstrated modest levels of antibacterial activity against MRSA, with MIC values of 16 μ g/mL (Figure S64).

3. Materials and Methods

3.1. Sample Collection

The medicinal plant *K. coccinea* was collected from a mountain ditch in Tongdao County, Huailua City, Hunan Province, China (E109°25'53'', N25°52'00''). The plant was identified by the Department of Chinese Pharmacy of the School of Pharmaceutical Sciences, Hunan University of Medicine.

3.2. Isolation of Endophytes

The separation methods used for endophytic actinomycetes are detailed in the Supplementary Materials.

3.3. Genomic DNA Extraction, 16S rRNA Gene Sequencing and Phylogenetic Tree Construction

S. sp. PH9030 was selected for cultivation in 50 mL of TSB medium. The mixture was agitated at 220 rpm for two days at 30 °C. The resulting mycelium biomass was then obtained by separating it via centrifugal precipitation. In accordance with the instructions provided by the manufacturer, the mycelium biomass that was collected was used in the process of extracting genomic DNA via the Ezup Column Bacteria Genomic DNA Purification Kit. Genomic DNA was extracted via conventional procedures [41]. The verified DNA was preserved at a temperature of -20 °C for future use. The 16S rRNA gene was amplified via the universal primer pair 27F/1492R under these conditions [42]. The resulting PCR products were subsequently cloned and sequenced [42]. The NCBI-BLAST database was used to perform sequence similarity searches and ascertain pairwise similarity values. The GenBank database has been updated with the partial sequences of the 16S rRNA gene that were obtained from *S. sp.* PH9030. Additionally, the accession code PP593435 was allocated to this sequence. A phylogenetic tree was created via the neighbor joining technique via MEGA 11.0 software. The 13 strains that were closest to each other at the genus level were chosen on the basis of the 16S rRNA sequence, which was compared with the database [43]. Bootstrap values (expressed as percentages of 1000 replications) over 50% are shown at branching nodes. The bar was 0.20 substitutions per nucleotide position.

3.4. General Methods

The equipment, including those used for optical rotation, HRESIMS, NMR and ECD, as well as the usual reagents used for chemical separation and biological assessment, were identical to those previously reported [32]. The details are listed in the Supplementary Materials.

3.5. Large-Scale Fermentation and Extraction

The *S. sp.* PH9030 strain was grown on MH16 (Table S1) agar plates and incubated at 30 °C to obtain spores. *S. sp.* PH9030 was subsequently grown in 250 mL Erlenmeyer flasks containing 50 mL sterile seed medium TSB and incubated at 30 °C on a rotary shaker (220 rpm) for 48 h. Finally, the seed culture (50 mL) was transferred into 2 L baffled Erlenmeyer flasks containing 500 mL sterile seed medium MH13 (Table S1) containing 4% microporous resins D1300 at 30 °C for 7 days. After fermentation, the culture (123 L) was filtered with EtOAc/MeOH (*v/v*, 1:1) (5 \times 3 L) to yield D1300 resins. The EtOAc/MeOH extract was subsequently evaporated in vacuo to afford 159.4 g of crude extract.

3.6. Isolation of Compounds 5–12

The EtOAc/MeOH extract fraction (159.4 g) was chromatographed on silica gel columns with petroleum/EtOAc (*v/v*, 19:1 → 9:1 → 7:3 → 1:1 → 3:7 → 1:9), EtOAc, EtOAc/MeOH (*v/v*, 9:1 → 7:3 → 1:1 → 3:7 → 1:9 → 0:1) to yield twenty combined fractions (Fr. A to T). Fr. K (1.459 g) was run through an MCI column (H₂O/MeOH, *v/v*, 9:1 → 4:1 → 7:3 → 3:2 → 1:1 → 2:3 → 7:13 → 3:7 → 1:3 → 1:4 → 1:9 → 0:1) to obtain five fractions altogether (Fr. K1 to K5). Fr. K3 (0.198 g) was separated by Sephadex LH-20 with MeOH as the mobile phase, obtaining three fractions altogether (Fr. K3-1 to Fr. K3-3). Fr. K3-1 (0.183 g) was run through an ODS column (H₂O/MeOH, *v/v*, 9:1 → 4:1 → 7:3 → 3:2 → 1:1 → 2:3 → 7:13 → 3:7 → 1:4 → 1:9 → 0:1) to obtain six fractions altogether (Fr. K3-1-1 to Fr. K3-1-6). Fr. K3-1-4 (0.114 g) was purified using semipreparative HPLC with 50% MeCN/H₂O (containing 0.1% formic acid) for 17 min at a flow rate of 3.0 mL/min to yield **5** (9.8 min, 2.797 mg) and **6** (11.1 min, 2.173 mg). Fr. G (10.872 g) was run through an MCI column (H₂O/MeOH, *v/v*, 9:1 → 4:1 → 7:3 → 3:2 → 1:1 → 2:3 → 3:7 → 1:4 → 1:9 → 0:1) to obtain ten fractions altogether (Fr. G1 to G10). Fr. G5 (0.097 g) was run through an ODS column (H₂O/MeOH, *v/v*, 9:1 → 4:1 → 7:3 → 3:2 → 1:1 → 2:3 → 3:7 → 1:4 → 1:9 → 0:1) to obtain six fractions altogether (Fr. G5-1 to Fr. G5-6). Fr. G5-4 (0.049 g) was purified using semipreparative HPLC with 70% MeCN/H₂O (containing 0.1% formic acid) for 14 min at a flow rate of 3.0 mL/min to yield **7** (13.2 min, 9.399 mg). Fr. G5-2 (0.008 g) was purified using semipreparative HPLC with 40% MeCN/H₂O (containing 0.1% formic acid) for 12 min at a flow rate of 3.0 mL/min to yield **9** (11.4 min, 0.952 mg). Fr. G7 (0.187 g) was run through an ODS column (H₂O/MeOH, *v/v*, 9:1 → 4:1 → 7:3 → 3:2 → 1:1 → 2:3 → 3:7 → 1:4 → 1:9 → 0:1) to obtain six fractions altogether (Fr. G7-1 to Fr. G7-6). Fr. G7-1 (0.016 g) was purified using semipreparative HPLC with 50% MeCN/H₂O (containing 0.1% formic acid) for 14 min at a flow rate of 3.0 mL/min to yield **10** (13.0 min, 0.957 mg). Fr. G7-4 (0.031 g) was purified using semipreparative HPLC with 50% MeCN/H₂O (containing 0.1% formic acid) for 15 min at a flow rate of 3.0 mL/min to yield **11** (14.5 min, 2.300 mg). Fr. R (10.020 g) was run through an ODS column (H₂O/MeOH, *v/v*, 19:1 → 9:1 → 4:1 → 7:3 → 3:2 → 1:1 → 2:3 → 3:7 → 1:4 → 1:9 → 1:19 → 0:1) to obtain ten fractions altogether (Fr. R1 to Fr. R10). Fr. R2 (0.191 g) was run through an MCI column (H₂O/MeOH, *v/v*, 9:1 → 17:3 → 4:1 → 7:3 → 3:2 → 1:1 → 2:3 → 3:7 → 1:4 → 1:9 → 0:1) to obtain ten fractions altogether (Fr. R2-1 to Fr. R2-10). Fr. R2-4 (0.050 g) was separated by Sephadex LH-20 with MeOH as the mobile phase to yield **8** (6.795 mg). Fr. D (9.675 g) was run through an MCI column (H₂O/MeOH, *v/v*, 19:1 → 9:1 → 4:1 → 7:3 → 3:2 → 1:1 → 2:3 → 3:7 → 1:4 → 1:9 → 0:1) to obtain three fractions altogether (Fr. D1 to D3). Fr. D3 (5.618 g) was separated by Sephadex LH-20 with MeOH as the mobile phase, obtaining three fractions altogether (Fr. D3-1 to Fr. D3-3). Fr. D3-2 (0.015 g) was purified using semipreparative HPLC with 55% MeCN/H₂O (containing 0.1% formic acid) for 12 min at a flow rate of 3.0 mL/min to yield **12** (11.2 min, 6.830 mg).

Naphthgeranine G (**5**)

Yellow powder; LC-UV (MeCN/H₂O/0.1% formic acid) λ_{max} 213.5, 265.5, 311.9, 389.6; $[\alpha]_{\text{D}}^{20.0}$ −276.67 (c 0.006, MeOH); ¹H, ¹³C and 2D NMR spectroscopic data are shown in Table 1 and Figures S4; HRESIMS *m/z* 355.1177 [M − H][−] (calcd for C₂₀H₁₉O₆, 355.1187).

3.7. ECD Calculation Methods

The ECD spectrum of **5** was calculated via the Gaussian 09 program [44]. The B3LYP/6-31G (d) level was used to optimize those configurations. With the CPCM model in methanol solution, the ECD spectrum was computed via TDDFT at the B3LYP/6-311+ +G (2d, p) level [45]. The details are provided in the Supplementary Materials.

3.8. α -Glucosidase Inhibition Assay

The Worawalai technique was employed to evaluate the inhibitory activity of **5–12** against α -glucosidase [Sigma-Aldrich (Shanghai) Trading Co., Ltd., Shanghai, China,

Product No. G5003] with minor modifications [46]. The levels of α -glucosidase were detected at 405 nm for a spectrophotometric in vitro α -glucosidase inhibitory activity test. The Supplementary Materials provide a detailed description of the reaction system.

3.9. Molecular Docking Analysis

The approach is outlined in the Supplementary Materials.

3.10. Molecular Dynamic Simulations

The approach is described in the Supplementary Materials.

3.11. Antibacterial Assay

The broth dilution method was used to determine the minimum inhibitory concentrations (MICs) [47]. The details are described in the Supplementary Materials.

4. Conclusions

In conclusion, a genus strain was identified from 30 strains of *Streptomyces* endophytic of *K. coccinea*, named *S. sp.* PH9030. An undescribed naphthoquinone analog, naphthgeranine G (**5**), together with seven known compounds, **6–12**, were isolated from *S. sp.* PH9030. NMR, HRESIMS and ECD spectra were used to establish the structures of all the compounds. Naphthgeranine G (**5**), 12-hydroxy-naphthgeranine A (**6**), naphthgeranine A (**7**) and phenazine-1-carboxamide (**9**) showed α -glucosidase inhibitory activities with IC₅₀ values of $66.4 \pm 6.7 \mu\text{M}$, $115.6 \pm 4.4 \mu\text{M}$, $185.9 \pm 0.2 \mu\text{M}$ and $105.4 \pm 10.5 \mu\text{M}$, respectively. Molecular docking and molecular dynamics further suggest that **5** is a potential α -glucosidase inhibitor. Evaluations of their inhibitory activities against *Staphylococcus aureus* ATCC 29213, MRSA, *Klebsiella pneumoniae* ATCC 13883 and *Pseudomonas aeruginosa* ATCC 9027 revealed that **9** and **12** both exhibited moderate antibacterial activity against MRSA, with MIC values of $16 \mu\text{g/mL}$. Considering the above results, the discovery of naphthoquinone and phenazine analogs enriches the secondary metabolites derived from endophytic *Streptomyces* of *K. coccinea* and, more importantly, provides lead compounds for the development of α -glucosidase inhibitors.

Supplementary Materials: The following supporting information can be downloaded at: <https://www.mdpi.com/article/10.3390/molecules29153450/s1>, Table S1: The media used in the experiment; Table S2: The activities of 18 strains; Table S3: Gibbs free energies and equilibrium populations of low-energy conformers of **5**; Table S4: Cartesian coordinates for the low-energy reoptimized random research conformers of **5** at B3LYP-D3(BJ)/6-31G* level of theory in methanol; Table S5: Antibacterial activity (MIC, $\mu\text{g/mL}$) of **5–12**; Table S6: Docking output of **5–12** and acarbose; Table S7: Antibacterial activity (MIC, $\mu\text{g/mL}$) of **5–12**; Figure S1: HPLC analysis of the culture broths from the *Streptomyces sp.* PH9001–PH9030; Figure S2: The Antibacterial activity of *Streptomyces sp.* PH9001–PH9030; Figure S3: The partial 16S rRNA gene sequences data of *Streptomyces sp.* PH9030; Figure S4: ¹H NMR spectrum of **5** in DMSO-*d*₆ (600 MHz); Figure S5: ¹³C NMR spectrum of **5** in DMSO-*d*₆ (150 MHz); Figure S6: DEPT-90 spectrum of **5**; Figure S7: DEPT-135 spectrum of **5**; Figure S8: HSQC spectrum of **5**; Figure S9: HMBC spectrum of **5**; Figure S10: ¹H–¹H COSY spectrum of **5**; Figure S11: NOESY spectrum of **5**; Figure S12: HRESIMS spectrum of **5**; Figure S13: UV spectrum of **5**; Figure S14: Optical rotation spectrum of **5**; Figure S15: ¹H NMR spectrum of **6** in DMSO-*d*₆ (600 MHz); Figure S16: ¹³C NMR spectrum of **6** in DMSO-*d*₆ (150 MHz); Figure S17: DEPT-90 spectrum of **6**; Figure S18: DEPT-135 spectrum of **6**; Figure S19: HSQC spectrum of **6**; Figure S20: HMBC spectrum of **6**; Figure S21: ¹H–¹H COSY spectrum of **6**; Figure S22: NOESY spectrum of **6**; Figure S23: HRESIMS spectrum of **6**; Figure S24: UV spectrum of **6**; Figure S25: ¹H NMR spectrum of **7** in DMSO-*d*₆ (600 MHz); Figure S26: ¹³C NMR spectrum of **7** in DMSO-*d*₆ (150 MHz); Figure S27: DEPT-135 spectrum of **7**; Figure S28: HSQC spectrum of **7**; Figure S29: HMBC spectrum of **7**; Figure S30: ¹H–¹H COSY spectrum of **7**; Figure S31: HRESIMS spectrum of **7**; Figure S32: UV spectrum of **7**; Figure S33: ¹H NMR spectrum of **8** in DMSO-*d*₆ (600 MHz); Figure S34: ¹³C NMR spectrum of **8** in DMSO-*d*₆ (150 MHz); Figure S35: DEPT-135 spectrum of **8**; Figure S36: HSQC spectrum of **8**; Figure S37: HMBC spectrum of **8**; Figure S38: HRESIMS spectrum of **8**; Figure S39: UV spectrum of **8**; Figure S40:

¹H NMR spectrum of **9** in DMSO-*d*₆ (600 MHz); Figure S41: ¹³C NMR spectrum of **9** in DMSO-*d*₆ (600 MHz); Figure S42: HRESIMS spectrum of **9**; Figure S43: UV spectrum of **9**; Figure S44: ¹H NMR spectrum of **10** in DMSO-*d*₆ (600 MHz); Figure S45: ¹³C NMR spectrum of **10** in DMSO-*d*₆ (150 MHz); Figure S46: HMBC spectrum of **10**; Figure S47: HRESIMS spectrum of **10**; Figure S48: UV spectrum of **10**; Figure S49: ¹H NMR spectrum of **11** in DMSO-*d*₆ (500 MHz); Figure S50: ¹³C NMR spectrum of **11** in DMSO-*d*₆ (125 MHz); Figure S51: DEPT-90 spectrum of **11**; Figure S52: DEPT-135 spectrum of **11**; Figure S53: HSQC spectrum of **11**; Figure S54: HMBC spectrum of **11**; Figure S55: ¹H-¹H COSY spectrum of **11**; Figure S56: NOESY spectrum of **11**; Figure S57: HRESIMS spectrum of **11**; Figure S58: UV spectrum of **11**; Figure S59: ¹H NMR spectrum of **12** in DMSO-*d*₆ (500 MHz); Figure S60: ¹³C NMR spectrum of **12** in DMSO-*d*₆ (125 MHz); Figure S61: HRESIMS spectrum of **12**; Figure S62: UV spectrum of **12**; Figure S63: Docking poses and interactions of acarbose with α-glucosidase (PDB ID: 2QMJ); Figure S64: 96-well plate assay of **5–12** against *Staphylococcus aureus* ATCC 29213 (A), MRSA (B), *Klebsiella pneumoniae* ATCC 13883 (C) and *Pseudomonas aeruginosa* ATCC 9027 (D) using the microbroth dilution method. Refs. [48–62] are listed in Supporting Materials.

Author Contributions: Conceptualization, formal analysis, funding acquisition, writing—original draft, writing—review and editing, H.P.; investigation, data acquisition, formal analysis, writing—original draft preparation, Q.M., Y.Z. and P.H.; formal analysis, writing—review and editing, Z.W. and G.W.; data acquisition, writing—review and editing, A.L., L.J. and H.Y.; investigation, data acquisition, T.J.; conceptualization, funding acquisition, J.L. and X.H. All authors have read and agreed to the published version of the manuscript.

Funding: This research was funded by the National Natural Science Foundation of China, under grant number 82274178 (to J.L.); the Hunan Provincial Natural Science Foundation of China, under grant number 2022JJ50294 (to H.P.); Hunan Provincial Department of Education Science Research Project, under grant number 22B1036 (to H.P.); the Hunan University of Medicine High-Level Talent Introduction Startup Funds, under grant number 202203 (to H.P.); the Wuxi Young Talent Program of Huaihua City Grant, under grant number 202104 (to J.L.); and the National Innovation and Entrepreneurship Training for University of PRC, under grant number 202212214002 (to Q.M.), S202312214006 (to Y.Z.) and S202312214004 (to Z.W.).

Institutional Review Board Statement: Not applicable.

Informed Consent Statement: Not applicable.

Data Availability Statement: Data generated in the process of this research are available in the Supporting Information.

Acknowledgments: We thank the Center for Advanced Research in CSU for the NMR experiments.

Conflicts of Interest: The authors declare no conflicts of interest.

References

1. Gheith, O.; Farouk, N.; Nampoory, N.; Halim, M.A.; Al-Otaibi, T. Diabetic Kidney Disease: World Wide Difference of Prevalence and Risk Factors. *J. Nephroarmacol.* **2016**, *5*, 49–56. [CrossRef]
2. GBD 2021 Diabetes Collaborators Global, Regional, and National Burden of Diabetes from 1990 to 2021, with Projections of Prevalence to 2050: A Systematic Analysis for the Global Burden of Disease Study 2021. *Lancet* **2023**, *402*, 203–234. [CrossRef]
3. Blahova, J.; Martiniakova, M.; Babikova, M.; Kovacova, V.; Mondockova, V.; Omelka, R. Pharmaceutical Drugs and Natural Therapeutic Products for the Treatment of Type 2 Diabetes Mellitus. *Pharmaceuticals* **2021**, *14*, 806. [CrossRef]
4. Derosa, G.; Maffioli, P. α-Glucosidase Inhibitors and Their Use in Clinical Practice. *Arch. Med. Sci.* **2012**, *8*, 899–906. [CrossRef]
5. Donald, L.; Pipite, A.; Subramani, R.; Owen, J.; Keyzers, R.A.; Taufa, T. *Streptomyces*: Still the Biggest Producer of New Natural Secondary Metabolites, a Current Perspective. *Microbiol. Res.* **2022**, *13*, 418–465. [CrossRef]
6. Schmidt, D.D.; Frommer, W.; Junge, B.; Müller, L.; Wingender, W.; Truscheit, E.; Schäfer, D. α-Glucosidase Inhibitors. New Complex Oligosaccharides of Microbial Origin. *Naturwissenschaften* **1977**, *64*, 535–536. [CrossRef]
7. Rockser, Y.; Wehmeier, U.F. The Gac-Gene Cluster for the Production of Acarbose from *Streptomyces Glaucescens* GLA.O—Identification, Isolation and Characterization. *J. Biotechnol.* **2009**, *140*, 114–123. [CrossRef]
8. Wang, Y.J.; Liu, L.L.; Wang, Y.S.; Xue, Y.P.; Zheng, Y.G.; Shen, Y.C. *Actinoplanes utahensis* ZJB-08196 Fed-Batch Fermentation at Elevated Osmolality for Enhancing Acarbose Production. *Bioresour. Technol.* **2012**, *103*, 337–342. [CrossRef]
9. Kameda, Y.; Asano, N.; Yoshikawa, M.; Takeuchi, M.; Yamaguchi, T.; Matsui, K.; Horii, S.; Fukase, H. Valiolamine, a New α-Glucosidase Inhibiting Aminocyclitol Produced by *Streptomyces hygroscopicus*. *J. Antibiot.* **1984**, *37*, 1301–1307. [CrossRef]

10. Ghani, U. Re-Exploring Promising α -Glucosidase Inhibitors for Potential Development into Oral Anti-Diabetic Drugs: Finding Needle in the Haystack. *Eur. J. Med. Chem.* **2015**, *103*, 133–162. [[CrossRef](#)]
11. Mackenzie, T.A.; Reyes, F.; Martínez, M.; González-Menéndez, V.; Sánchez, I.; Genilloud, O.; Tormo, J.R.; Ramos, M.C. Naphthoquinone Derivatives from *Angustimassarina populi* CF-097565 Display Anti-Tumour Activity in 3D Cultures of Breast Cancer Cells. *Molecules* **2024**, *29*, 425. [[CrossRef](#)]
12. Efeoglu, C.; Selcuk, O.; Demir, B.; Sahin, E.; Sari, H.; Türkeş, C.; Demir, Y.; Nural, Y.; Beydemir, Ş. New Naphthoquinone Thiazole Hybrids as Carbonic Anhydrase and Cholinesterase Inhibitors: Synthesis, Crystal Structure, Molecular Docking, and Acid Dissociation Constant. *J. Mol. Struct.* **2024**, *1301*, 137365. [[CrossRef](#)]
13. Matsuda, Y.; Abe, I. Biosynthesis of Fungal Meroterpenoids. *Nat. Prod. Rep.* **2015**, *33*, 26–53. [[CrossRef](#)]
14. Kashi, M.E.; Ghorbani, M.; Badibostan, H.; Seidel, V.; Hosseini, S.H.; Asili, J.; Shakeri, A.; Sahebkar, A. Antimicrobial and Cytotoxic Naphthoquinones from Microbial Origin: An Updated Review. *Mini Rev. Med. Chem.* **2024**, *24*, 844–862. [[CrossRef](#)] [[PubMed](#)]
15. Murray, L.A.M.; McKinnie, S.M.K.; Moore, B.S.; George, J.H. Meroterpenoid Natural Products from *Streptomyces* Bacteria—the Evolution of Chemoenzymatic Syntheses. *Nat. Prod. Rep.* **2020**, *37*, 1334–1366. [[CrossRef](#)] [[PubMed](#)]
16. Komiyama, K.; Funayama, S.; Anraku, Y.; Ishibashi, M.; Takahashi, Y.; Omura, S. Novel Antibiotics, Furaquinocins A and B. Taxonomy, Fermentation, Isolation and Physico-Chemical and Biological Characteristics. *J. Antibiot.* **1990**, *43*, 247–252. [[CrossRef](#)]
17. Pathirana, C.; Jensen, P.R.; Fenical, W. Marinone and Debromomarinone: Antibiotic Sesquiterpenoid Naphthoquinones of a New Structure Class from a Marine Bacterium. *Tetrahedron Lett.* **1992**, *33*, 7663–7666. [[CrossRef](#)]
18. Guttenberger, N.; Blankenfeldt, W.; Breinbauer, R. Recent Developments in the Isolation, Biological Function, Biosynthesis, and Synthesis of Phenazine Natural Products. *Bioorg. Med. Chem.* **2017**, *25*, 6149–6166. [[CrossRef](#)]
19. Blankenfeldt, W.; Parsons, J.F. The Structural Biology of Phenazine Biosynthesis. *Curr. Opin. Struct. Biol.* **2014**, *29*, 26–33. [[CrossRef](#)]
20. Kankanamge, S.; Khalil, Z.G.; Capon, R.J. Tepuazines A–E: Phenazine Glycosides from a Venezuelan Quartz-Rich (Tepui) Cave Soil-Derived *Streptomyces virginiae* CMB-CA091. *J. Nat. Prod.* **2024**, *87*, 1084–1091. [[CrossRef](#)]
21. Laursen, J.B.; Nielsen, J. Phenazine Natural Products: Biosynthesis, Synthetic Analogues, and Biological Activity. *Chem. Rev.* **2004**, *104*, 1663–1686. [[CrossRef](#)]
22. Noakes, F.F.; Smitten, K.L.; Maple, L.E.C.; Bernardino de la Serna, J.; Robertson, C.C.; Pritchard, D.; Fairbanks, S.D.; Weinstein, J.A.; Smythe, C.G.W.; Thomas, J.A. Phenazine Cations as Anticancer Theranostics. *J. Am. Chem. Soc.* **2024**, *146*, 12836–12849. [[CrossRef](#)]
23. Liu, K.; Li, Z.; Liang, X.; Xu, Y.; Cao, Y.; Wang, R.; Li, P.; Li, L. Biosynthesis and Genetic Engineering of Phenazine-1-Carboxylic Acid in *Pseudomonas chlororaphis* Lzh-T5. *Front. Microbiol.* **2023**, *14*, 1186052. [[CrossRef](#)]
24. Mahdally, N.H.; ElShiekh, R.A.; Thissera, B.; Eltahir, A.; Osama, A.; Mokhtar, M.; Elhosseiny, N.M.; Kashef, M.T.; Magdeldin, S.; El Halawany, A.M.; et al. Dihydrophenazine: A Multifunctional New Weapon That Kills Multidrug-Resistant *Acinetobacter baumannii* and Restores Carbapenem and Oxidative Stress Susceptibilities. *J. Appl. Microbiol.* **2024**, *135*, 1xae100. [[CrossRef](#)]
25. Xun, W.; Gong, B.; Liu, X.; Yang, X.; Zhou, X.; Jin, L. Antifungal Mechanism of Phenazine-1-Carboxylic Acid against *Pestalotiopsis kenyana*. *Int. J. Mol. Sci.* **2023**, *24*, 11274. [[CrossRef](#)]
26. Song, Y.; Li, Q.Y.; Cong, M.J.; Pang, X.Y.; Chen, B.; Liu, Y.H.; Liao, L.; Wang, J.F. Cytotoxic Phenazine and Antiallergic Phenoxazine Alkaloids from an Arctic *Nocardioopsis dassonvillei* SCSIO 502F. *Nat. Prod. Bioprospect.* **2023**, *13*, 41. [[CrossRef](#)]
27. Borrero, N.V.; Bai, F.; Perez, C.; Duong, B.Q.; Rocca, J.R.; Jin, S.; Huigens Iii, R.W. Phenazine Antibiotic Inspired Discovery of Potent Bromophenazine Antibacterial Agents against *Staphylococcus aureus* and *Staphylococcus epidermidis*. *Org. Biomol. Chem.* **2014**, *12*, 881–886. [[CrossRef](#)]
28. Kennedy, R.K.; Naik, P.R.; Veena, V.; Lakshmi, B.S.; Lakshmi, P.; Krishna, R.; Sakthivel, N. 5-Methyl Phenazine-1-Carboxylic Acid: A Novel Bioactive Metabolite by a Rhizosphere Soil Bacterium That Exhibits Potent Antimicrobial and Anticancer Activities. *Chem. Biol. Interact.* **2015**, *231*, 71–82. [[CrossRef](#)]
29. Yang, Y.P.; Hussain, N.; Zhang, L.; Jia, Y.Z.; Jian, Y.Q.; Li, B.; Iqbal Choudhary, M.; Rahman, A.U.; Wang, W. *Kadsura coccinea*: A Rich Source of Structurally Diverse and Biologically Important Compounds. *Chin. Herb. Med.* **2020**, *12*, 214–223. [[CrossRef](#)]
30. Dong, J.J.; Ma, J.Y.; Yang, W.Y.; Cai, W.; Wu, W.H. Characterization of the Volatile Profile and Its Estrogenic Activity in *Kadsura coccinea* Fruit. *J. Ethnopharmacol.* **2023**, *309*, 116341. [[CrossRef](#)]
31. Jiang, L.; Pu, H.; Xiang, J.; Su, M.; Yan, X.; Yang, D.; Zhu, X.; Shen, B.; Duan, Y.; Huang, Y. Huanglongmycin A-C, Cytotoxic Polyketides Biosynthesized by a Putative Type II Polyketide Synthase from *Streptomyces* sp. CB09001. *Front. Chem.* **2018**, *6*, 254. [[CrossRef](#)]
32. Jiang, L.; Pu, H.; Qin, X.; Liu, J.; Wen, Z.; Huang, Y.; Xiang, J.; Xiang, Y.; Ju, J.; Duan, Y.; et al. Syn-2, 3-Diols and Anti-Inflammatory Indole Derivatives from *Streptomyces* sp. CB09001. *Nat. Prod. Res.* **2021**, *35*, 144–151. [[CrossRef](#)]
33. Pu, H.; Jiang, T.; Peng, D.; Xia, J.; Gao, J.; Wang, Y.; Yan, X.; Huang, X.; Duan, Y.; Huang, Y. Degradation of Mirubactin to Multiple Siderophores with Varying Fe(III) Chelation Properties. *Org. Biomol. Chem.* **2022**, *20*, 5066–5070. [[CrossRef](#)]
34. Lu, C.; Yang, C.H.; Xu, Z. Three Naphthoquinones from *Streptomyces* sp. XZYN-4. *Rec. Nat. Prod.* **2016**, *10*, 430–440.
35. Wessels, P.; Göhr, A.; Zeeck, A.; Drautz, H.; Zähner, H. Metabolic Products of Microorganisms, 260. Naphthgeranines, New Naphthoquinone Antibiotics from *Streptomyces* sp. *J. Antibiot.* **1991**, *44*, 1013–1018. [[CrossRef](#)]

36. Wang, Z.; Yang, F.X.; Liu, C.; Wang, L.; Qi, Y.; Cao, M.; Guo, X.; Li, J.; Huang, X.; Yang, J.; et al. Isolation and Biosynthesis of Phenazine-Polyketide Hybrids from *Streptomyces* sp. KIB-H483. *J. Nat. Prod.* **2022**, *85*, 1324–1331. [[CrossRef](#)]
37. Jayatilake, G.S.; Thornton, M.P.; Leonard, A.C.; Grimwade, J.E.; Baker, B.J. Metabolites from an Antarctic Sponge-Associated Bacterium, *Pseudomonas aeruginosa*. *J. Nat. Prod.* **1996**, *59*, 293–296. [[CrossRef](#)]
38. Geiger, A.; Keller-Schierlein, W.; Brandl, M.; Zähler, H. Metabolites of Microorganisms. 247. Phenazines from *Streptomyces antibioticus*, Strain Tü 2706. *J. Antibiot.* **1988**, *41*, 1542–1551. [[CrossRef](#)]
39. Zhu, X.; Wu, Q.; Li, J. Research Progress of Phenazine-1-carboxylic Acid and Its Analogue. *Chin. J. Org. Chem.* **2019**, *39*, 2744. [[CrossRef](#)]
40. Ye, C.; Zhang, R.; Dong, L.; Chi, J.; Huang, F.; Dong, L.; Zhang, M.; Jia, X. α -Glucosidase Inhibitors from Brown Rice Bound Phenolics Extracts (BRBPE): Identification and Mechanism. *Food Chem.* **2022**, *372*, 131306. [[CrossRef](#)]
41. Kieser, T.; Bibb, M.; Chater, K.; Butter, M.; Hopwood, D.; Bittner, M.; Buttner, M. *Practical Streptomyces Genetics: A Laboratory Manual*; John Innes Centre Foundation: Norwich, UK, 2000.
42. Rainey, F.A.; Ward-Rainey, N.; Kroppenstedt, R.M.; Stackebrandt, E. The Genus *Nocardiopsis* Represents a Phylogenetically Coherent Taxon and a Distinct Actinomycete Lineage: Proposal of *Nocardiopsaceae* fam. nov. *Int. J. Syst. Bacteriol.* **1996**, *46*, 1088–1092. [[CrossRef](#)] [[PubMed](#)]
43. Kumar, S.; Stecher, G.; Li, M.; Niyaz, C.; Tamura, K. MEGA X: Molecular Evolutionary Genetics Analysis across Computing Platforms. *Mol. Biol. Evol.* **2018**, *35*, 1547–1549. [[CrossRef](#)] [[PubMed](#)]
44. Frisch, M.J.; Trucks, G.W.; Schlegel, H.B.; Scuseria, G.E.; Robb, M.A.; Cheeseman, J.R.; Scalmani, G.; Barone, V.; Mennucci, B.; Petersson, G.A.; et al. *Gaussian 09, Revision C.01*; Gaussian Inc.: Wallingford, CT, USA, 2010.
45. Bruhn, T.; Schaumlöffel, A.; Hemberger, Y.; Bringmann, G. SpecDis: Quantifying the Comparison of Calculated and Experimental Electronic Circular Dichroism Spectra. *Chirality* **2013**, *25*, 243–249. [[CrossRef](#)] [[PubMed](#)]
46. Xu, X.T.; Deng, X.Y.; Chen, J.; Liang, Q.M.; Zhang, K.; Li, D.L.; Wu, P.P.; Zheng, X.; Zhou, R.P.; Jiang, Z.Y.; et al. Synthesis and Biological Evaluation of Coumarin Derivatives as α -Glucosidase Inhibitors. *Eur. J. Med. Chem.* **2020**, *189*, 112013. [[CrossRef](#)] [[PubMed](#)]
47. Wiegand, I.; Hilpert, K.; Hancock, R.E.W. Agar and Broth Dilution Methods to Determine the Minimal Inhibitory Concentration (MIC) of Antimicrobial Substances. *Nat. Protoc.* **2008**, *3*, 163–175. [[CrossRef](#)] [[PubMed](#)]
48. Neese, F. The ORCA Program System. *WIREs Comput. Mol. Sci.* **2012**, *2*, 73–78. [[CrossRef](#)]
49. Stephens, P.J.; Harada, N. ECD Cotton Effect Approximated by the Gaussian Curve and Other Methods. *Chirality* **2010**, *22*, 229–233. [[CrossRef](#)] [[PubMed](#)]
50. Trott, O.; Olson, A.J. AutoDock Vina: Improving the Speed and Accuracy of Docking with a New Scoring Function, Efficient Optimization, and Multithreading. *J. Comput. Chem.* **2010**, *31*, 455–461. [[CrossRef](#)] [[PubMed](#)]
51. Sanner, M.F. Python: A Programming Language for Software Integration and Development. *J. Mol. Graph. Model.* **1999**, *17*, 57–61. [[PubMed](#)]
52. Morris, G.M.; Huey, R.; Lindstrom, W.; Sanner, M.F.; Belew, R.K.; Goodsell, D.S.; Olson, A.J. AutoDock4 and AutoDockTools4: Automated Docking with Selective Receptor Flexibility. *J. Comput. Chem.* **2009**, *30*, 2785–2791. [[CrossRef](#)]
53. Salomon-Ferrer, R.; Case, D.A.; Walker, R.C. An Overview of the Amber Biomolecular Simulation Package. *WIREs Comput. Mol. Sci.* **2013**, *3*, 198–210. [[CrossRef](#)]
54. Sagui, C.; Darden, T.A. Molecular Dynamics Simulations of Biomolecules: Long-Range Electrostatic Effects. *Annu. Rev. Biophys. Biomol. Struct.* **1999**, *28*, 155–179. [[CrossRef](#)]
55. Kräutler, V.; Van Gunsteren, W.F.; Hünenberger, P.H. A Fast SHAKE Algorithm to Solve Distance Constraint Equations for Small Molecules in Molecular Dynamics Simulations. *J. Comput. Chem.* **2001**, *22*, 501–508. [[CrossRef](#)]
56. Larini, L.; Mannella, R.; Leporini, D. Langevin Stabilization of Molecular-Dynamics Simulations of Polymers by Means of Quasisymplectic Algorithms. *J. Chem. Phys.* **2007**, *126*. [[CrossRef](#)] [[PubMed](#)]
57. Hou, T.; Wang, J.; Li, Y.; Wang, W. Assessing the Performance of the MM/PBSA and MM/GBSA Methods. 1. The Accuracy of Binding Free Energy Calculations Based on Molecular Dynamics Simulations. *J. Chem. Inf. Model.* **2011**, *51*, 69–82. [[CrossRef](#)]
58. Chen, Y.; Zheng, Y.; Fong, P.; Mao, S.; Wang, Q. The Application of the MM/GBSA Method in the Binding Pose Prediction of FGFR Inhibitors. *Phys. Chem. Chem. Phys.* **2020**, *22*, 9656–9663. [[CrossRef](#)]
59. Genheden, S.; Ryde, U. The MM/PBSA and MM/GBSA Methods to Estimate Ligand-Binding Affinities. *Expert Opin. Drug Discov.* **2015**, *10*, 449–461. [[CrossRef](#)]
60. Rastelli, G.; Rio, A.D.; Degliesposti, G.; Sgobba, M. Fast and Accurate Predictions of Binding Free Energies Using MM-PBSA and MM-GBSA. *J. Comput. Chem.* **2010**, *31*, 797–810. [[CrossRef](#)]
61. Nguyen, H.; Roe, D.R.; Simmerling, C. Improved Generalized Born Solvent Model Parameters for Protein Simulations. *J. Chem. Theory Comput.* **2013**, *9*, 2020–2034. [[CrossRef](#)]
62. Weiser, J.; Shenkin, P.S.; Still, W.C. Approximate Atomic Surfaces from Linear Combinations of Pairwise Overlaps (LCPO). *J. Comput. Chem.* **1999**, *20*, 217–230. [[CrossRef](#)]

Disclaimer/Publisher's Note: The statements, opinions and data contained in all publications are solely those of the individual author(s) and contributor(s) and not of MDPI and/or the editor(s). MDPI and/or the editor(s) disclaim responsibility for any injury to people or property resulting from any ideas, methods, instructions or products referred to in the content.